Identification of a novel ADAMTS9/GON-1 function for protein transport from the ER to the Golgi

Sawako Yoshina[a,b,c], Kenjiro Sakaki[a], Aki Yonezumi-Hayashi[a,b,*], Keiko Gengyo-Ando[a,b,†], Hideshi Inoue[c], Yuichi Iino[d], and Shohei Mitani[a,b,e]

[a]Department of Physiology, Tokyo Women's Medical University School of Medicine, Tokyo 162-8666, Japan; [b]Core Research for Evolutional Science and Technology, Japan Science and Technology Agency, Tokyo, 102-0076 Japan; [c]School of Life Sciences, Tokyo University of Pharmacy and Life Sciences, Hachioji 192-0392, Japan; [d]Department of Biochemistry and Biophysics, University of Tokyo, Tokyo 113-0033, Japan; [e]Institute for Integrated Medical Sciences, Tokyo Women's Medical University, Tokyo 162-8666, Japan

ABSTRACT **A disintegrin-like and metalloprotease with thrombospondin type I motif (ADAMTS9) is a member of the secreted metalloprotease family that is believed to digest extracellular matrix (ECM) proteins outside of cells. Its *Caenorhabditis elegans* orthologue, GON-1, is involved in ECM degradation and is required for gonad morphogenesis. ADAMTS9 and GON-1 have similar domain structures, and both have a unique C-terminal domain called the "GON domain," whose function remains unknown. Here we show that down-regulation of human ADAMTS9 and *C. elegans* GON-1 results in the inhibition of protein transport from the endoplasmic reticulum (ER) to the Golgi. This phenotype was rescued by the expression of the GON domain localizing in the ER in human cells and *C. elegans*. We propose a novel function of ADAMTS9 and GON-1 in the ER that promotes protein transport from the ER to the Golgi. This function is GON-domain dependent but protease activity independent.**

Monitoring Editor
Anne Spang
University of Basel

Received: Oct 14, 2011
Revised: Feb 14, 2012
Accepted: Mar 6, 2012

INTRODUCTION

The A disintegrin-like and metalloprotease with thrombospondin type I motif (ADAMTS) family comprises secreted zinc metalloproteases with a precisely ordered modular organization that includes at least one thrombospondin type I repeat (Kuno *et al.*, 1997; Hurskainen *et al.*, 1999; Clark *et al.*, 2000). ADAMTS9 localizes extracellularly or on the cell surface and cleaves large, aggregating proteoglycans such as aggrecan and versican (Somerville *et al.*, 2003). Similar to most zymogens, the ADAMTS9 protease domain contains an N-terminal propeptide. The propeptide is believed to have a role in maintaining enzyme latency, and excision of the propeptide activates ADAMTS9. The ADAMTS9 propeptide is processed by furin at the cell surface (Somerville *et al.*, 2003) and is necessary for localization to the cell surface (Koo *et al.*, 2007). ADAMTS9 mRNA is widely expressed, especially during embryonic development in both humans and mice (Somerville *et al.*, 2003; Jungers *et al.*, 2005).

In humans, an ADAMTS9 gene variant in the 5′-upstream region (rs4607103) is associated with type 2 diabetes (Grarup *et al.*, 2008; Zeggini *et al.*, 2008), and this allele results in reduced insulin-stimulated glucose uptake (Boesgaard *et al.*, 2009). The molecular mechanisms underlying the effect of ADAMTS9 on the peripheral insulin action and risk of diabetes, however, are unknown. In mice, an ADAMTS9-null allele is early embryonic lethal (Silver *et al.*, 2008), suggesting that ADAMTS9 plays an essential role in organism survival, although the molecular mechanisms of ADAMTS9 involvement during embryogenesis are unknown. GON-1 is the *Caenorhabditis elegans* orthologue of ADAMTS9 and is required for distal tip cell (DTC) migration during gonad morphogenesis. GON-1 contributes to degradation of the basement membrane or the processing

This article was published online ahead of print in MBoC in Press (http://www.molbiolcell.org/cgi/doi/10.1091/mbc.E11-10-0857) on March 14, 2012.

Present addresses: *Department of Allergy and Rheumatology, Graduate School of Medicine and Faculty of Medicine, University of Tokyo, Tokyo 113-8655, Japan; †Saitama University Brain Science Institute, Saitama 338-8570, Japan.

Address correspondence to: Shohei Mitani (mitani1@research.twmu.ac.jp).

Abbreviations used: AAT, α1-antitrypsin; ADAMTS, A disintegrin-like and metalloprotease with thrombospondin type I motif; DTC, distal tip cell; ECM, extracellular matrix; ER, endoplasmic reticulum; GPI, glycosylphosphatidylinositol; NHK, null Hong Kong; PRL, prolactin; RNAi, RNA interference; ssVenus, secreted soluble Venus; TM, transmembrane; VSVG, vesicular stomatitis virus glycoprotein.

of extracellular cues required for cell migration by its protease activity (Blelloch *et al.*, 1999). It is of interest that membranes accumulate within the cytoplasm in DTC of *gon-1* mutants (Blelloch *et al.*, 1999). This phenotype is not predicted by the known protease functions of GON-1 and ADAMTS-family proteases (Porter *et al.*, 2005). Thus these previous reports suggest that GON-1 and ADAMTS9 have an additional function.

Here we report on the novel function of ADAMTS9 and GON-1, which are required for the protein secretory pathway from the endoplasmic reticulum (ER) to the Golgi in both *C. elegans* and human cells. It is surprising that this novel function depends on the GON domain without protease activity, and the GON domain plays a role in the ER but not extracellularly. The GON domain exists at the C-terminus of ADAMTS9, ADAMTS20, and GON-1 and in a number of GON-domain proteins in metazoans, suggesting that its role has broad biological significance. This is the first report of the GON-domain function, which is important for protein transport from the ER to the Golgi.

RESULTS

Gonad proliferation defects in a *gon-1* mutant are associated with abnormalities in ER structure and function and the ER stress response

A member of the ADAMTS-like metalloprotease family is encoded by *gon-1*, which is expressed in DTCs and body wall muscle cells and functions in extracellular matrix (ECM) remodeling in *C. elegans* (Jones and Riley, 2005). Depletion of GON-1 results in gonad proliferation defects and aberrant membrane morphology in hermaphrodite DTCs (Blelloch *et al.*, 1999). We confirmed this phenotype using RNA interference (RNAi) of *gon-1* [*gon-1(RNAi)*] in wild-type animals and a *gon-1* mutant (*tm3146*) (Figure 1A and Supplemental Figure S1). *gon-1(tm3146)* harbors a deletion that removes the protease domain, and a termination codon is introduced by a neighboring short insertion (Supplemental Figure S2).

We examined possible changes in the organelle structures of DTC in the *gon-1* reduction-of-function background to gain insights into the accumulation of the intracellular membrane. We generated transgenic strains that harbor a DTC-specific, *lag-2* promoter–driven cytochrome b5—a putative ER protein—fused to Venus. As expected, a fluorescence signal was observed around the nuclei of the DTCs in wild-type animals (Figure 1B, left). Treatment of the same transgenic strain by *gon-1(RNAi)* or introduction of the same transgene into the *gon-1(tm3146)* background resulted in a large and deformed green fluorescent protein (GFP)–positive structure in DTCs. The deformed fluorescence signals were observed as a few circular structures that were closely apposed to each other. The circular structures were also visible in differential interference contrast (DIC) images (Figure 1B, arrowhead). This phenotype might correspond to the extensive expansion of the membrane structure observed by electron microscopy (see Figure 1B, middle and right, Figure 3A later in the paper, and Supplemental Figure S1). The same results were observed when Venus-SP12 was used as another ER marker (Poteryaev *et al.*, 2005; (Supplemental Figure S3). The expression patterns of other organelle markers were not greatly changed by *gon-1(RNAi)* (Supplemental Figure S4). An ER-containing autophagosome (ERA)-like structure was also observed by electron microscopy (Supplemental Figure S1). ERA-like structures were reported to appear upon ER dysfunction (Bernales *et al.*, 2006).

We next evaluated whether protein secretion was impaired in *gon-1(RNAi)* because the ER structure was abnormal. The protein secretion activity of DTCs was examined based on the distribution of secreted soluble Venus (ssVenus) expressed in DTCs (Fares and Greenwald, 2001). Accumulation of Venus fluorescence was observed in DTCs of almost all of the transgenic animals treated with *gon-1(RNAi)* or in the *gon-1(tm3146)* background (see Figure 1C, middle and right, and Figure 3A later in the paper).

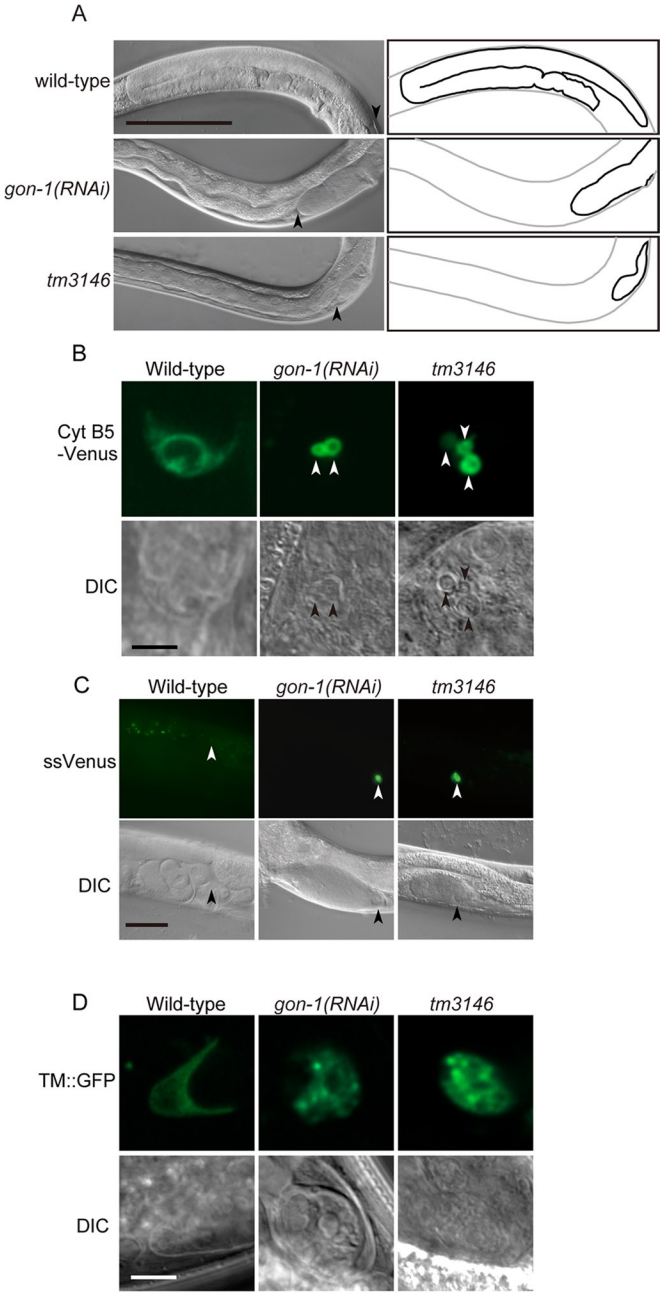

FIGURE 1: *gon-1(tm3146)* has an aberrant morphology of the ER and secretion defects. (A) In *gon-1* mutants and *gon-1(RNAi)* animals, gonadal arm extension did not occur. Arrowheads indicate the position of the tip of the gonad. The schematic drawings (right) indicate the morphology of the gonad. Scale bar, 100 μm. (B) ER morphology analyzed by an ER marker, cytochrome b5-Venus. Confocal fluorescence images drastically changed in animals treated with *gon-1(RNAi)* and *gon-1(tm3146)* mutants (top). Arrowheads indicate abnormal ER morphology. Bottom, the differential interference contrast (DIC) images. Scale bar, 5 μm. (C) Protein secretion from DTC was blocked in animals with *gon-1(RNAi)* and *gon-1(tm3146)* mutants (top). Bottom, the DIC images. Scale bar, 50 μm. (D) Transportation analyzed by a plasma membrane protein marker. Confocal fluorescence images changed in animals treated with *gon-1(RNAi)* and *gon-1(tm3146)* mutants (top). Bottom, the DIC images. Scale bar, 5 μm.

We then evaluated whether *gon-1* is necessary for the transportation of a plasma membrane protein and a glycosylphosphatidylinositol (GPI)-anchored protein. We generated transgenic worms expressing a *lag-2* promoter–driven enhanced GFP (EGFP) fused with the transmembrane (TM) domain of T01F10.1a (TM-EGFP) as a plasma membrane protein and yellow fluorescent protein (YFP)–GPI as a GPI-anchored protein. In wild-type animals, TM-EGFP and YFP-GPI localized to the plasma membrane (Figure 1C, left, and Supplemental Figure S5A, left). Punctate accumulation of TM-EGFP was observed in DTCs when the transgenic animals were treated by *gon-1(RNAi)* or in the *gon-1(tm3146)* background (Figure 1D, middle and right). The YFP-GPI signal accumulated in DTCs when transgenic animals were treated with *gon-1(RNAi)* (Supplemental Figure S5A, right). ER dysfunction in body wall muscle cells in the *gon-1(tm3146)* background was examined by evaluating protein secretion in transgenic worms harboring *arIs37*, which expressed and secreted soluble GFP from body wall muscles to the pseudocoelom. The secreted GFP in the pseudocoelom was endocytosed and accumulated in coelomocytes in wild-type animals (Supplemental Figure S5B, left, arrowhead), as previously reported (Fares and Greenwald, 2001). On the other hand, bright fluorescence was observed in the body wall muscle cells of *gon-1(tm3146)* mutants (Supplemental Figure S5B, right). We also examined the distribution of TM-EGFP expressed in body wall muscle cells. In wild-type animals, TM-EGFP mainly localized to the plasma membrane (Supplemental Figure S5C, left). In contrast, depletion of *gon-1* led to the punctate accumulation of TM-EGFP in body wall muscle cells (Supplemental Figure S5C, right), indicating that GON-1 is also required for TM-EGFP transport in body wall muscle cells.

The BiP protein, an ER-stress sensor, is induced when ER functions are impaired in mammalian cells. To determine whether the homologue in the nematode (*hsp-4*) is also induced in *gon-1(RNAi)*–treated animals, we used a transgenic allele *zcIs4* (Calfon *et al.*, 2002) harboring a transcriptional fusion reporter of *phsp-4::gfp*. In wild-type animals, GFP expression was not observed in DTCs (Supplemental Figure S6A, left). By contrast, *gon-1(RNAi)* induced GFP expression in DTCs (Supplemental Figure S6A, right).

To more directly evaluate the disturbance of ER functions, we performed reverse transcription-PCR (RT-PCR) analysis of *xbp-1*. XBP-1 is an important molecule for the unfolded protein response (UPR) in cells. Under ER stress conditions, *xbp-1* mRNA is processed by unconventional splicing, which results in the removal of an intron and a translational frame shift (Schroder and Kaufman, 2005), causing the conversion of the premature unspliced *xbp-1* (*xbp-1(U)*) to the spliced *xbp-1* (*xbp-1(S)*). The amount of *xbp-1*(S) mRNA was increased in *gon-1(RNAi)* animals (Supplemental Figure S6B), although the possibility that *xbp-1* was induced indirectly in other tissues could not be excluded because *xbp-1* might also exist in other cells. We generated transgenic worms that expressed a *lag-2* promoter–driven, Venus-fused *xbp-1* cDNA (*xbp-1(Δ81)::Venus*) to test whether the *xbp-1* splicing observed indeed occurs in DTCs. *xbp-1(Δ81)::Venus* is detected in DTCs only when the frame-switch splicing on *xbp-1* mRNA occurs upon ER stress. *gon-1(RNAi)* indeed induced XBP-1(*Δ81)*::Venus protein in DTCs (Supplemental Figure S6, C and D).

To examine the relationship between ER function and gonad proliferation and migration, we depleted oligosaccharyltransferase (*T12A2.2*) using RNAi. Oligosaccharyltransferase is essential for N-linked glycosylation in the ER (Dempski and Imperiali, 2002). Therefore, knockdown of this gene should mimic the treatment of animals with tunicamycin, which is a chemical inhibitor of N-linked glycosylation and a typical ER stress–inducing reagent. Gonad proliferation was also highly disturbed by RNAi knockdown of the *T12A2.2* gene in N2 worms, as in *gon-1*–mutant animals (Supplemental Figure S7). These results suggest that down-regulation of ER function accounts for some of the gonadal defects.

The GON domain localizes to the ER and is important for maintaining functions of the DTC

Other *gon-1*–mutant alleles—*q518* and *e1254*—retained the protease domain but also showed severe gonad morphogenesis defects (Blelloch and Kimble, 1999) and abnormal ER morphology in almost all DTCs (Supplemental Figure S8). We therefore evaluated which portion of the GON-1 protein is necessary for the structure and function of the ER in DTC. *q518* has a stop codon in front of the thrombospondin domain, and *e1254* has a stop codon within the thrombospondin domain (Supplemental Figure S2). Transgenic animals that expressed various truncated forms of *gon-1* and *plag-2::C31E10.7::Venus* in the wild-type or the *gon-1(tm3146)* mutant backgrounds were generated, and ER morphology and gonad proliferation were observed (Figures 2A and 3). We defined ER structure as abnormal when the ER had at least one bright fluorescent circular structure with a diameter of 1 μm or larger (Figure 3A). ER morphology was normal in 97% of wild-type animals, in only 5% of the *gon-1(tm3146)* mutants, and in only 10% of the *tm3146;tmEx*[*plag-2::gon-1(N-TSP12)*] mutants, in which the GON domain was absent. The incidence of normal ER morphology did not differ significantly between *gon-1(tm3146)* and *tm3146;tmEx*[*plag-2::gon-1(N-TSP12)*] ($p > 0.1$), and thus *plag-2::gon-1(N-TSP12)* did not rescue the ER morphology. ER morphology was normal in 81% of the *tm3146;tmEx*[*plag-2::gon-1(sig_GON)*] mutants, which had a signal sequence and the GON domain. The incidence of normal ER morphology differed significantly between *gon-1(tm3146)* and *tm3146;tmEx*[*plag-2::gon-1(sig_GON)*] animals ($p < 0.05$), indicating that *plag-2::gon-1(sig_GON)* rescued the ER morphology. ER morphology in *tm3146;tmEx*[*plag-2::gon-1(sig_GON)::KDEL*], which had the signal sequence, the GON domain, and the ER retention signal KDEL, was normal in 92% of the animals. The incidence of normal ER morphology was significantly different between *gon-1(tm3146)* and *tm3146;tmEx*[*plag-2::gon-1(sig_GON)::KDEL*] ($p < 0.05$), indicating that *plag-2::gon-1(sig_GON)::KDEL* rescued the ER morphology. ER morphology of *tm3146;tmEx*[*plag-2::gon-1(sig_Pro_GON)*], which had the signal sequence, the Pro domain, and the GON domain, was normal in 92% of the animals. The incidence of normal ER morphology was significantly different between *gon-1(tm3146)* and *tm3146;tmEx*[*plag-2::gon-1(sig_Pro_GON)*] ($p < 0.05$), indicating that *plag-2::gon-1(sig_Pro_GON)* rescued the ER morphology. ER morphology in *tm3146;tmEx*[*plag-2::gon-1(sig_GON), pmyo-3::gon-1(FL)*], which expressed a fusion protein of the signal sequence and the GON domain in DTCs and expressed the full-length GON-1 protein in muscle, was normal in 98% of the animals. The incidence of normal ER morphology was significantly different between *gon-1(tm3146)* and *tm3146;tmEx*[*plag-2::gon-1(sig_GON), pmyo-3::gon-1(FL)*] ($p < 0.05$), indicating that *plag-2::gon-1(sig_GON), pmyo-3::gon-1(FL)* rescued the ER morphology. ER morphology in *tm3146;tmEx*[*plag-2::gon-1(E425A)*], which had a Glu-425–to–Ala substitution in the active center of the metalloprotease but retained the GON domain, was normal in 77% of the animals. The incidence of normal ER morphology was significantly different between *gon-1(tm3146)* and *tm3146;tmEx*[*plag-2::gon-1(E425A)*] ($p < 0.05$), indicating that *plag-2::gon-1(E425A)* rescued the ER morphology. ER morphology in *tm3146;tmEx*[*plag-2::gon-1(sig_GON_Venus)*], which expressed a fusion protein containing

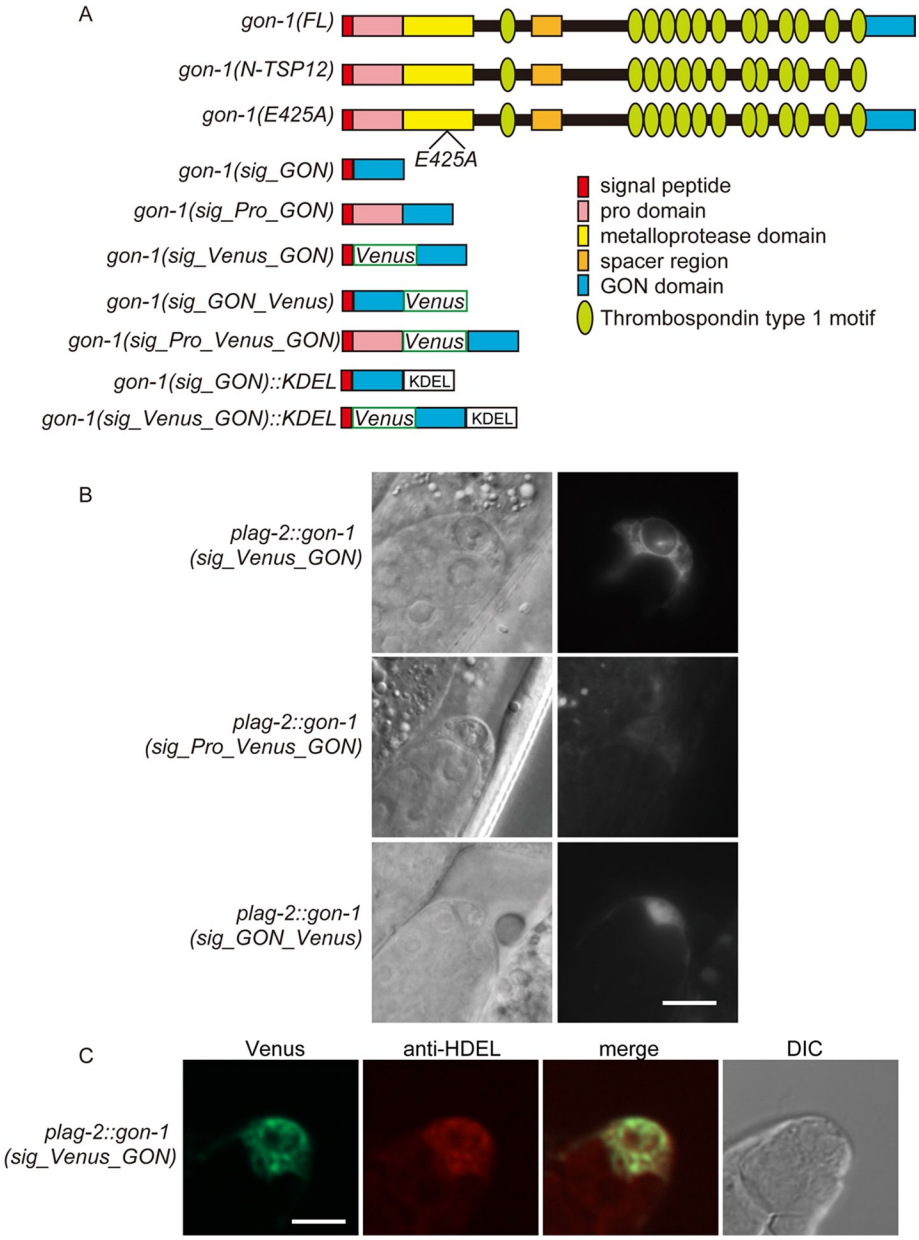

FIGURE 2: Expression of the GON domain is localized in the ER. (A) Domains and deletion constructs of GON-1. Each domain is shown by a colored box or oval. FL, full length; GON, the GON domain; KDEL, artificially added ER-retention signal; Pro, prodomain; Sig, signal peptide; TSP, thrombospondin. (B) *gon-1(sig_Venus_GON)* fluorescence localized to the ER in *C. elegans*, whereas *gon-1(sig_GON_Venus)* fluorescence was diffusely observed in the cytoplasm of DTC. *gon-1(sig_Pro_Venus_GON)* fluorescence was observed faintly in the DTC. Scale bar, 5 μm. (C) *gon-1(sig_Venus_GON)* localizes to the ER in the DTC. Immunofluorescence observation with an antibody against the ER-retention signal HDEL was performed on DTCs expressing *gon-1(sig_Venus_GON)*. Scale bar, 5 μm.

Venus at the C terminus of *sig_GON*, was normal in 25% of the animals. *plag-2::gon-1(sig_GON_Venus)* had a weaker rescue activity than did *plag-2::gon-1(sig_GON)*. The incidence of normal ER morphology was significantly different between *gon-1(tm3146)* and *tm3146;tmEx*[*plag-2::gon-1(sig_GON_Venus)*] ($p < 0.05$). The ER morphology in *tm3146;tmEx*[*plag-2::gon-1(sig_Venus_GON)*], which expressed a fusion protein in which Venus was fused to the N terminus of the GON domain, was normal in 84% of the animals. The incidence of normal ER morphology was significantly different between *gon-1(tm3146)* and *tm3146;tmEx*[*plag-2::gon-1(sig_Venus_GON)*] ($p < 0.05$), indicating that *plag-2::gon-1(sig_Venus_GON)* rescued the ER morphology. The ER morphology in *tm3146;tmEx*[*plag-2::gon-1(sig_Venus_GON)::KDEL*], which expressed a fusion protein in which a KDEL-tag was fused to the C terminus of *sig_Venus_GON*, was normal in 92% of the animals. The incidence of normal ER morphology was significantly different between *gon-1(tm3146)* and *tm3146;tmEx*[*plag-2::gon-1(sig_Venus_GON)::KDEL*] ($p < 0.05$), indicating that *plag-2::gon-1(sig_Venus_GON)::KDEL* rescued the ER morphology. The ER morphology in *tm3146;tmEx*[*plag-2::gon-1(sig_Pro_Venus_GON)*], which expressed a fusion protein in which Venus was fused between the Pro domain and the GON domain, was normal in 89% of the animals. The incidence of normal ER morphology differed significantly between *gon-1(tm3146)* and *tm3146;tmEx*[*plag-2::gon-1(sig_Venus_GON)*] ($p < 0.05$), indicating that *plag-2::gon-1(sig_Pro_Venus_GON)* rescued the ER morphology. ER morphology in *tm3146;tmEx*[*pmyo-3::gon-1(FL)*], which expressed GON-1 in muscles but not in the DTCs, was normal in 14% of the animals. The incidence of normal ER morphology did not differ significantly between *gon-1(tm3146)* and *tm3146;tmEx*[*pmyo-3::gon-1(FL)*] ($p > 0.1$), indicating that *pmyo-3::gon-1(FL)* did not rescue the ER morphology. These observations were confirmed with two additional alleles. ER morphology in transgenic strains harboring *plag-2::gon-1(sig_GON)* was rescued, but that in transgenic strains harboring *plag-2::gon-1(N-TSP12)* was not rescued in either the *gon-1(q518)* or *gon-1(e1254)* background (Supplemental Figure S8).

Because muscle expression of GON-1 results in the growth and expansion of gonadal tissues but not elongated gonads in the *gon-1(q518)* mutant (Blelloch and Kimble, 1999), we classified gonad proliferation as either "enlarged gonad" or "elongated gonad" (Figure 3B) according to the criteria for gonad proliferation described previously (Blelloch and Kimble, 1999). *tm3146;tmEx*[*plag-2::gon-1(N-TSP12)*] did not rescue gonad proliferation ($p > 0.1$). On the other hand, transgenic animals harboring a *lag-2* promoter–driven transgene that contained the GON domain, except for *tm3146;tmEx*[*plag-2::gon-1(sig_GON_Venus)*], rescued gonad proliferation ($p < 0.05$; Figures 2 and 3B). The gonads of *tm3146;tmEx*[*plag-2::gon-1(sig_GON)*] were enlarged in 20% of the animals. The gonads of *tm3146;tmEx*[*plag-2::gon-1(sig_GON)::KDEL*] were enlarged in 58% of the animals. This result indicates that *plag-2::gon-1(sig_GON)::KDEL* had a higher rescue activity than *plag-2::gon-1(sig_GON)*. The gonads of *tm3146;tmEx*[*plag-2::gon-1(sig_Venus_GON)*] were enlarged and elongated in 33 and 4% of the animals,

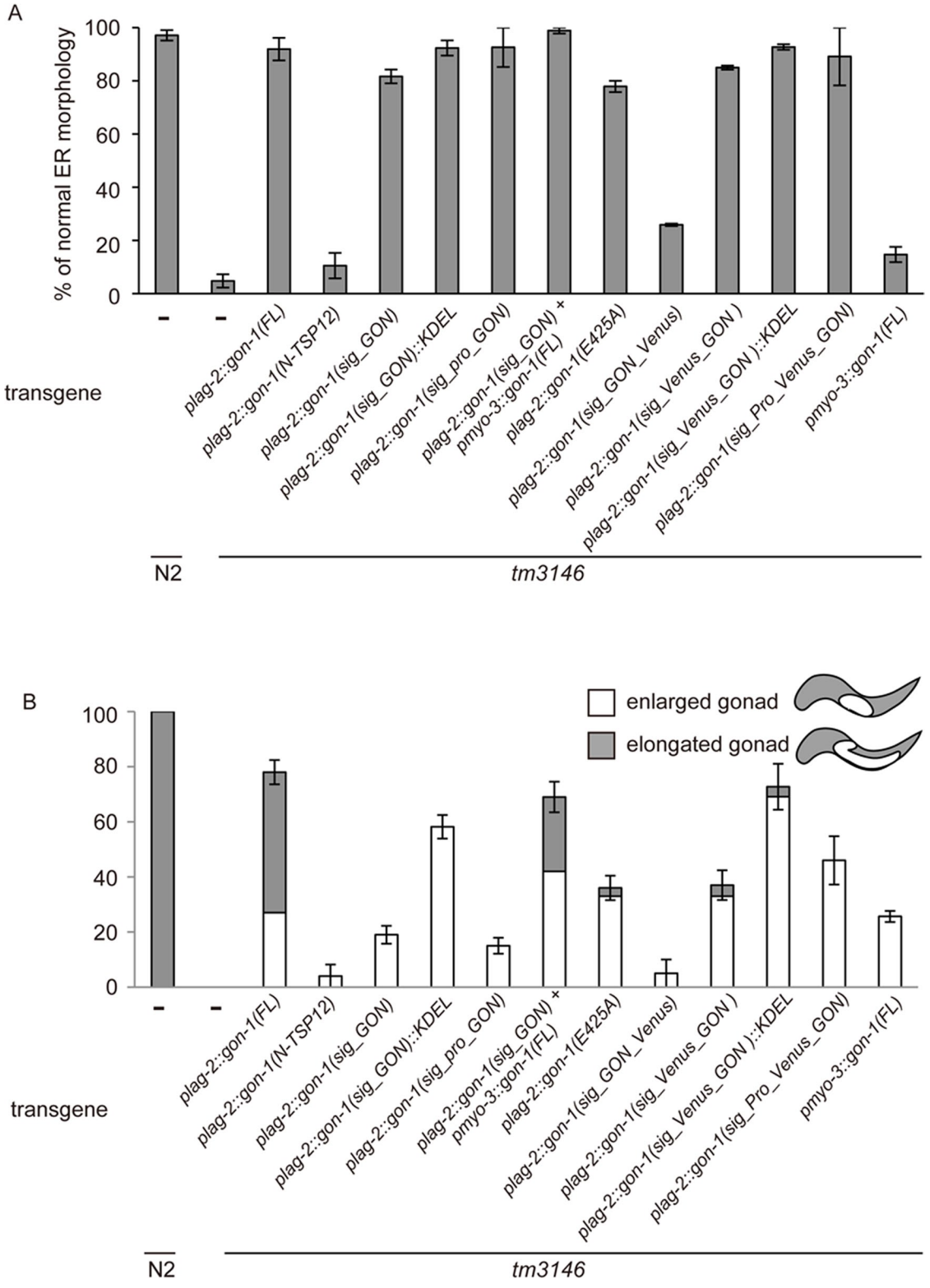

FIGURE 3: The GON domain is important to operate in the ER for maintaining the ER morphology and gonadal proliferation in *C. elegans*. (A) Rescue activities of the ER morphology by various *gon-1* transgenes are shown. The transgenes used are the same as those in Figure 2. Genetic backgrounds (N2 or *tm3146*) are shown at the bottom. The graph represents the combined results of five independent experiments (n > 40 for each experiment). Bars represent mean ± SE. (B) Rescue activities of gonadal proliferation by various *gon-1* transgenes are shown. Transgenes used are the same as those in A and in Figure 2. Populations of enlarged gonads and elongated gonads are shown with the white boxes and shaded boxes, respectively. Genetic backgrounds (N2 or *tm3146*) are shown at the bottom. The graph represents the combined results of five independent experiments (n > 40 for each experiment). Bars represent mean ± SE.

respectively. The gonads of *tm3146;tmEx*[*plag-2::gon-1(sig_Venus_GON)::KDEL*] were enlarged and elongated in 69 and 4% of the animals, respectively, indicating that *plag-2::gon-1(sig_Venus_GON)::KDEL* had a higher rescue activity than *plag-2::gon-1(sig_Venus_GON)*.

To investigate the underlying mechanisms of such different rescue activities among *tm3146;tmEx*[*plag-2::gon-1(sig_Venus_GON)*], *tm3146;tmEx*[*plag-2::gon-1(sig_Pro_Venus_GON)*], and *tm3146;tmEx*[*plag-2::gon-1(sig_GON_Venus)*], we compared the localization of *plag-2::gon-1(sig_Venus_GON)* and *tm3146;tmEx*[*plag-2::gon-1(sig_Pro_Venus_GON)*], which had strong rescue activities, and *plag-2::gon-1(sig_GON_Venus)*, which had a weak rescue activity. When *gon-1(sig_Venus_GON)* was expressed in DTCs, a mesh-like structure was observed. On the other hand, *gon-1(sig_GON_Venus)* localized diffusely to the cytoplasm of DTCs (Figure 2B). When *gon-1(sig_Pro_Venus_GON)* was expressed in DTCs, a mesh-like structure was faintly observed. To further analyze the localization of *gon-1(sig_Venus_GON)* in DTCs, we immunostained dissected DTCs expressing *plag-2::gon-1(sig_Venus_GON)* with an anti-HDEL antibody that stains the ER in *C. elegans* (Pourkarimi *et al*. 2012). *gon-1(sig_Venus_GON)* colocalized with the anti-HDEL immunoreactivity (Figure 2C).

These findings suggest that *gon-1* functions both inside and outside of the cell. On the basis of these data, we propose that localization of the GON domain in the ER is important for intracellular function and that localization of *gon-1*, both inside and outside of the cell, is important for gonad proliferation.

Deformation of ER structure, inhibition of protein secretion, and frame-switch splicing of *xbp-1* are induced after GON domain inactivation

We observed the time course of the morphological changes in the ER and the inhibition of protein secretion by chromophore-assisted light inactivation of the GON domain (Bulina *et al*., 2006). We created a light-inactivatable fusion protein of the KillerRed and GON domain by substituting Venus in *gon-1(sig_Venus_GON)* with KillerRed. We generated transgenic animals that expressed *lag-2* promoter–driven *gon-1(sig_KillerRed_GON)* in the *gon-1(tm3146)* mutant background (Figure 4A). This transgene also rescued the ER morphology, accumulation of ssVenus, and splicing of *xbp-1* in DTCs in the absence of green-light illumination. When the animals are illuminated with green light, the GON domain fused to KillerRed is inactivated (Bulina *et al*., 2006). Thus we could inactivate the GON domain by illuminating the animals with green light.

We generated transgenic animals expressing *lag-2* promoter–driven *gon-1(sig_KillerRed_GON)* and an ER marker in *gon-1(tm3146)* mutants and evaluated ER morphology using fluorescence microscopy after green-light irradiation for 0, 2, 5, 10, and 24 h. Light-induced inactivation of the GON domain affected the ER morphology after 24 h of green-light exposure. In contrast, in the dark control, abnormal ER morphology was rarely observed (Figure 4, B and C).

In transgenic animals expressing *lag-2* promoter–driven *gon-1(sig_KillerRed_GON)* and ssVenus in *gon-1(tm3146)* mutants, ssVenus accumulation in the DTCs was examined after irradiation with green light for 0, 2, 5, 10, and 24 h. Accumulation of ssVenus induced by light inactivation of the GON domain was observed after irradiation for 2 h. In the dark control, there was only slight accumulation of ssVenus (Figure 4, D and E).

We generated transgenic animals expressing *lag-2* promoter–driven *gon-1(sig_KillerRed_GON)* and *xbp-1(Δ81)*::Venus in the *gon-1(tm3146)* mutant background and observed the accumulation of XBP-1(Δ81)::Venus in DTCs after green-light irradiation for 0, 2, 5, 10, and 24 h. Fluorescence was detected in DTCs only when frame-switch splicing on *xbp-1* mRNA occurred upon ER stress. Light inactivation of the GON domain induced the frame-switch splicing of *xbp-1* after 5 h of green-light exposure. In the dark control, the amount of frame-switch–spliced *xbp-1* remained at the background level (Supplemental Figure S9).

Depletion of ADAMTS9 in a mammalian cell line inhibits transport from the ER to the Golgi

To determine whether the *gon-1*–like protein function is conserved in mammalian cells, we performed small interfering RNA (siRNA)–mediated knockdown of ADAMTS9, a human homologue of GON-1, in HEK293 cells. Staining with an ER-Tracker showed that ADAMTS9 depletion induced deformation of the ER morphology (Figure 5A). ER-Tracker–positive globular structures were observed in ADAMTS9 siRNA–treated cells but rarely in the control siRNA–treated cells. To confirm the abnormal ER structures in the ADAMTS9 siRNA–treated cells, we examined the ER structure with electron microscopy. We observed tightly stacked whirling membrane patterns in ADAMTS9-depleted cells but not in the control siRNA–treated cells (Supplemental Figure S10).

Vesicular transport was observed using the temperature-sensitive vesicular stomatitis virus glycoprotein (VSVG; ts045) fused to GFP. In this experimental system, VSVG-GFP first accumulates in the ER when cultured at 40°C, and when the temperature is shifted to 32°C, the molecules are translocated from the ER to the plasma membrane through the Golgi. Localization of VSVG-GFP was evaluated by immunostaining with an anti-GM130 antibody or an anti-KDEL antibody. As expected, in the cells treated with control siRNA or ADAMTS9 siRNA, when cultured at 40°C, VSVG-GFP fluorescence localized to the ER, as shown by colocalization of anti-KDEL antibody staining (Supplemental Figure S11), but not to the Golgi, as shown by colocalization of anti-GM130 antibody staining (Figure 5B). After 20 min at the permissive temperature, in the cells treated with control siRNA, VSVG-GFP fluorescence localized to the Golgi in 76% of the cells, based on the colocalization of anti-GM130 antibody staining (Figure 5, B and C), but not in the ER, based on the colocalization of anti-KDEL antibody staining (Supplemental Figure S11). VSVG-GFP fluorescence localized to both the Golgi and the ER in 22% of the cells. At later time points, the VSVG-GFP was eventually translocated to the plasma membrane (unpublished data). In contrast, in ADAMTS9 siRNA–treated cells, 20 min after transfer to the permissive temperature, VSVG-GFP fluorescence localized to the Golgi in 18% of the cells and to both the Golgi and the ER in 27% of the cells. VSVG-GFP fluorescence localized to the ER in 55% of the cells, as shown by colocalization of anti-KDEL antibody staining (Figure 5C and Supplemental Figure S11). VSVG-GFP fluorescence did not colocalize with anti-GM130 antibody immunoreactivity in 55% of the cells (Figure 5B). These results indicate that ADAMTS9 knockdown caused the accumulation of VSVG-GFP within the ER 20 min after shifting the temperature to 32°C in HEK293 cells (Figure 5, B and C, and Supplemental Figure S11).

To investigate other phenotypes in mammalian cells, we examined whether ADAMTS9 is required for the secretory function in HEK293 cells. Knockdown of ADAMTS9 caused the accumulation of GFP fused with the prolactin (PRL) secretory signal within the cells (Supplemental Figure S12). We also examined whether frame-switch splicing of XBP1 is observed in ADAMTS9 siRNA–treated mammalian cells. This was indeed the case in HEK293 cells (Supplemental Figure S13A). Although the cell morphology changed a little,

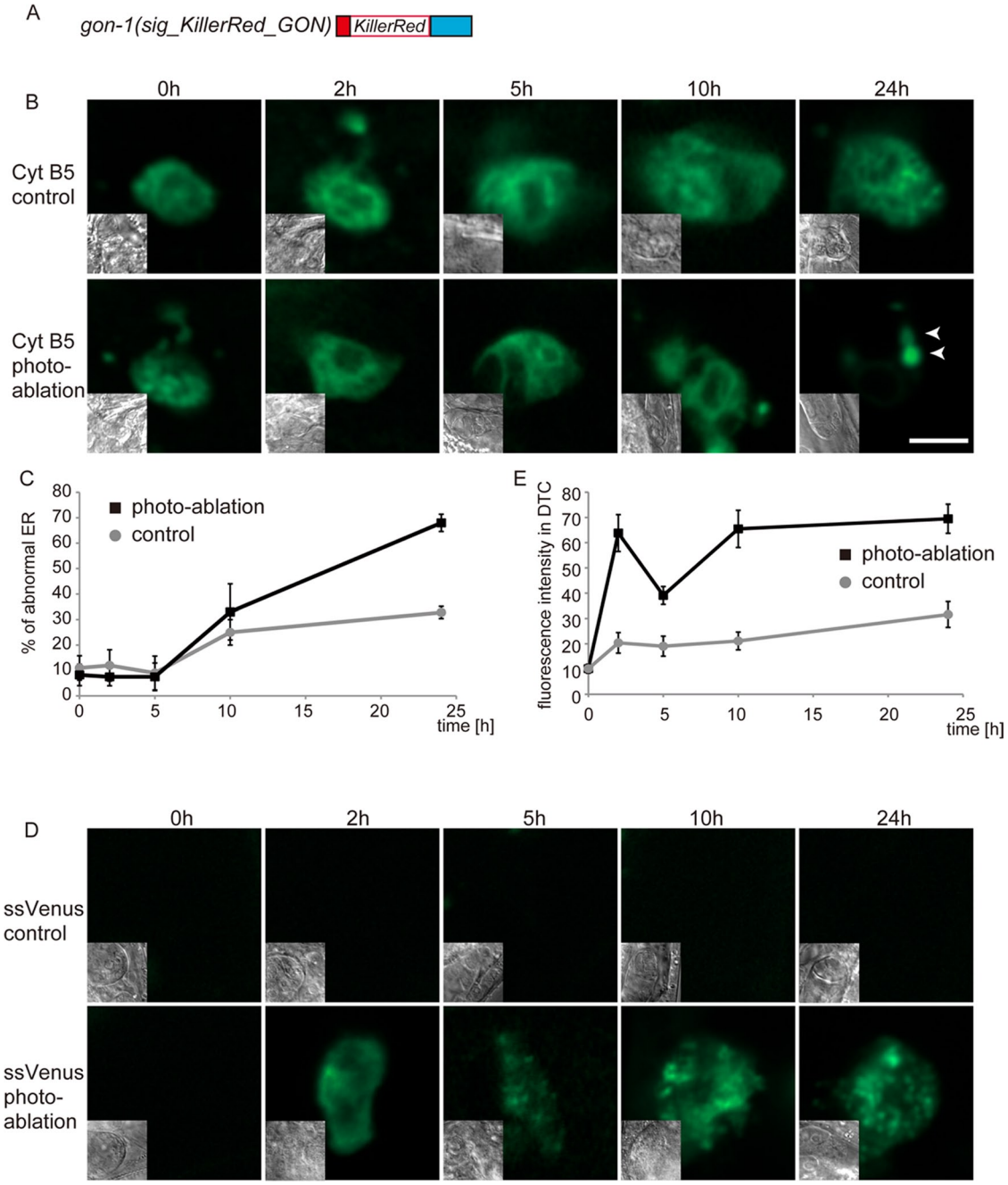

FIGURE 4: Time course of alteration of ER structure and protein secretion from DTC after KillerRed-mediated, light-induced inactivation of the GON domain. (A) A schematic diagram of the fusion protein used in B–E and Supplemental Figure S8. Domains are indicated as described in Figure 2A. (B) ER morphology of *gon-1* mutants that expressed *plag-2::gon-1(sig_KillerRed_GON)* and *plag-2::C31E10.7::Venus* was observed at the indicated time points by confocal fluorescence microscopy after illumination with a green light (photoablation) or not (control). ER morphology changed dramatically between 10 and 24 h after irradiation, as shown by arrowheads. Scale bar, 5 μm. (C) Quantification of the results in B. The graph represents the combined results of six independent experiments (n > 100 for each experiment). Bars represent mean ± SE. (D) Accumulation of ssVenus within DTC in *gon-1* mutants that expressed *plag-2::gon-1(sig_KillerRed_GON)* and *plag-2::ssVenus* was observed at the indicated time points by confocal fluorescence microscopy after illumination with a green light (photoablation) or not (control). ssVenus accumulation in DTC was observed after 2 h of irradiation. (E) Quantification of the results in D. The graph represents the combined results of five independent experiments (n > 90 for each experiment). Bars represent mean ± SE.

becoming rounder (Figure 5A), and too strong ER stress may cause apoptosis, we examined cell viability of ADAMTS9 siRNA–treated HEK293 cells. The cell viability was unchanged between control and ADAMTS9 siRNA–treated cells (Supplemental Figure S13B).

To investigate whether the GON domain alone could rescue the ER-to-Golgi transport phenotype in HEK293 cells, as observed in *C. elegans*, we transfected VSVG-GFP and *gon-1(sig_GON)* into HEK293 cells treated with ADAMTS9 siRNA or control siRNA. In this

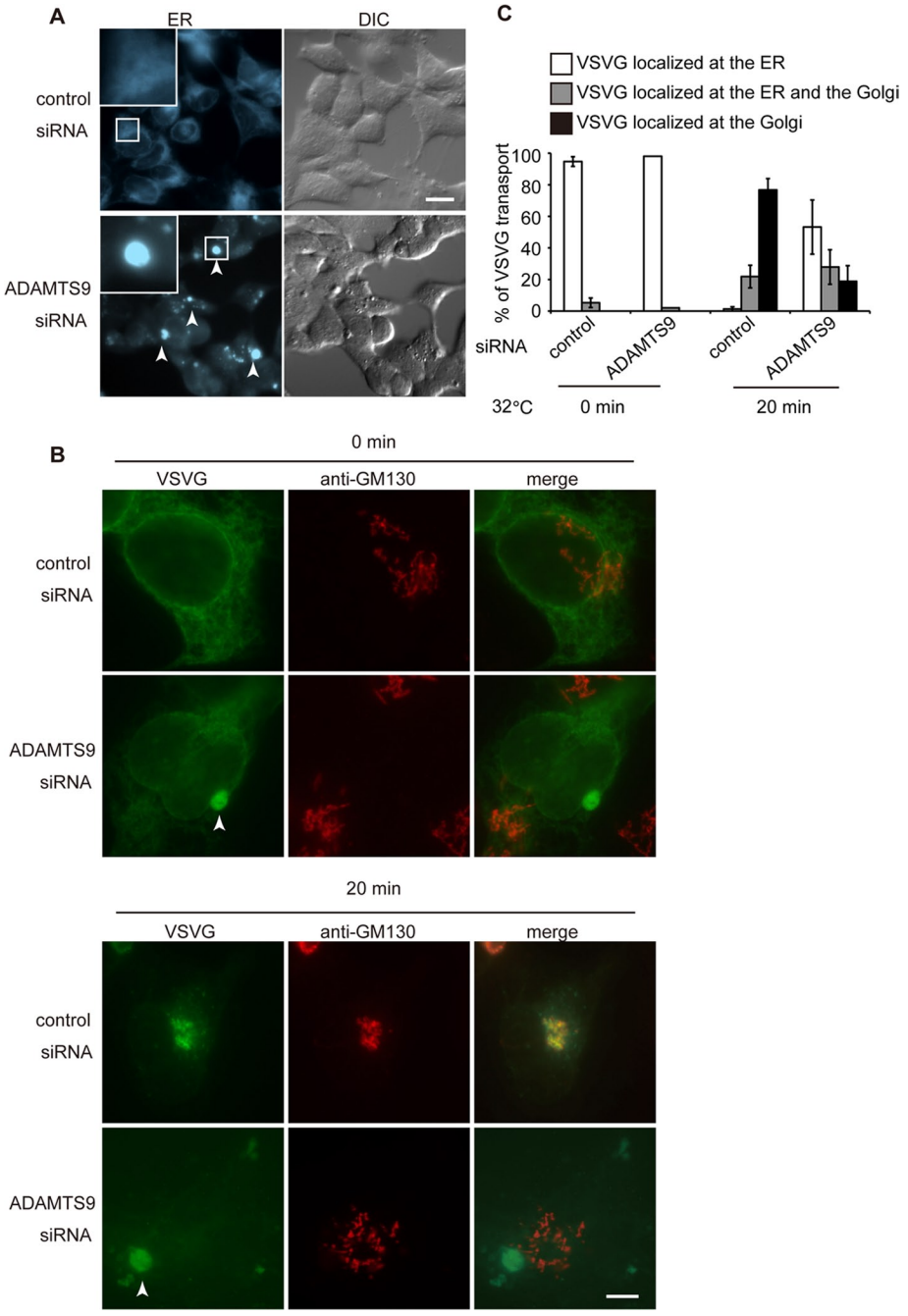

FIGURE 5: Knockdown of ADAMTS9 inhibited ER to Golgi transport in mammalian cells. (A) The shrunken ER was observed in the cells treated with ADAMTS9 siRNA (arrowheads). The siRNA-treated cells were stained with an ER-tracker (left), and DIC images of the same field are shown (right). Scale bar, 20 μm. (B) VSVG-expressing cells were incubated for 16 h at 40°C and then shifted to 32°C. The cells were fixed at the indicated time points following transfer to the permissive temperature. The Golgi apparatus was labeled by an anti-GM130 antibody (middle). VSVG-GFP images were merged with those of the Golgi (right). VSVG-GFP transport from the ER to the Golgi was inhibited in the cells in which siRNA–mediated knockdown of ADAMTS9 was performed. Arrowheads indicate the shrunken ER in ADAMTS9-knockdown cells. Scale bar, 5 μm. (C) Quantification of the VSVG transports. The graph represents the combined results of four independent experiments (n > 50 for each experiment). Bars represent mean ± SE.

siRNA-plasmid transfection experiment, because the GON-domain nucleotide sequences are very different between human and *C. elegans*, the transfected siRNA should not knock down the GON domain mRNA from the rescue plasmid. These cells were stained with an anti-GM130 antibody or an anti-KDEL antibody, and localization of VSVG-GFP was evaluated. At 40°C, VSVG-GFP accumulated in the ER, as shown by colocalization of anti-KDEL antibody staining in 100% of the *gon-1(sig_GON)*–introduced and control siRNA–treated cells and in 100% of the *gon-1(sig_GON)*–introduced ADAMTS9 siRNA–treated cells (Figure 6, A and B, and Supplemental Figure S14). After 20 min at the permissive temperature, VSVG-GFP localized to the Golgi, as shown by colocalization of anti-GM130 antibody staining in 85% of the *gon-1(sig_GON)*–introduced and control siRNA–treated cells. After 20 min at the permissive temperature, VSVG-GFP localized to the Golgi in 83% of the *gon-1(sig_GON)*–introduced and ADAMTS9 siRNA–treated cells (Figure 6, A and B). VSVG-GFP did not localize to the ER, as shown by colocalization of anti-KDEL antibody staining in these cells (Supplemental Figure S14). These observations support the idea that the GON domain, but not the protease activity, is required for cargo transport from the ER to the Golgi in HEK293 cells.

We next analyzed the subcellular localization of various GON-domain proteins in mammalian cells to determine protein structure–function relationship. To do this, we transfected *gon-1(sig_GON_Venus)*, *gon-1(sig_Venus_GON)*, ADAMTS9(sig_GON_Venus), or ADAMTS9(sig_Venus_GON) into HEK293 cells and observed Venus fluorescence localization. When HEK293 cells were transfected with plasmids expressing *gon-1(sig_Venus_GON)* and ADAMTS9(sig_Venus_GON), fluorescence was observed in the ER, as shown by colocalization with the calnexin immunoreactivity. In contrast, *gon-1(sig_GON_Venus)* and ADAMTS9(sig_GON_Venus) localized diffusely throughout the cytoplasm (Supplemental Figure S15). These findings are similar to the localization of the GON domain in the nematode. Taken together, these observations of HEK293 cells were similar to the phenotypes found in the nematode.

Because cargo molecules accumulated in the ER, and ER stress was induced under the ADAMTS9-depleted condition, we evaluated whether secretory proteins are normally O-linked glycosylated in the Golgi and degraded normally by the proteasome system. We expressed α1-antitrypsin (AAT) to monitor secretion in HEK293 cells treated with or without ADAMTS9 siRNA and found that ADAMTS9 knockdown caused the accumulation of AAT within the cells and a reduction of AAT in the medium (Supplemental Figure S16, A–C), similar to the accumulation of the prolactin-GFP fusion protein described earlier. We used the enzyme endoglycosidase H (Endo H), which removes N-linked glycosylation, but not O-linked glycosylation, from proteins in the

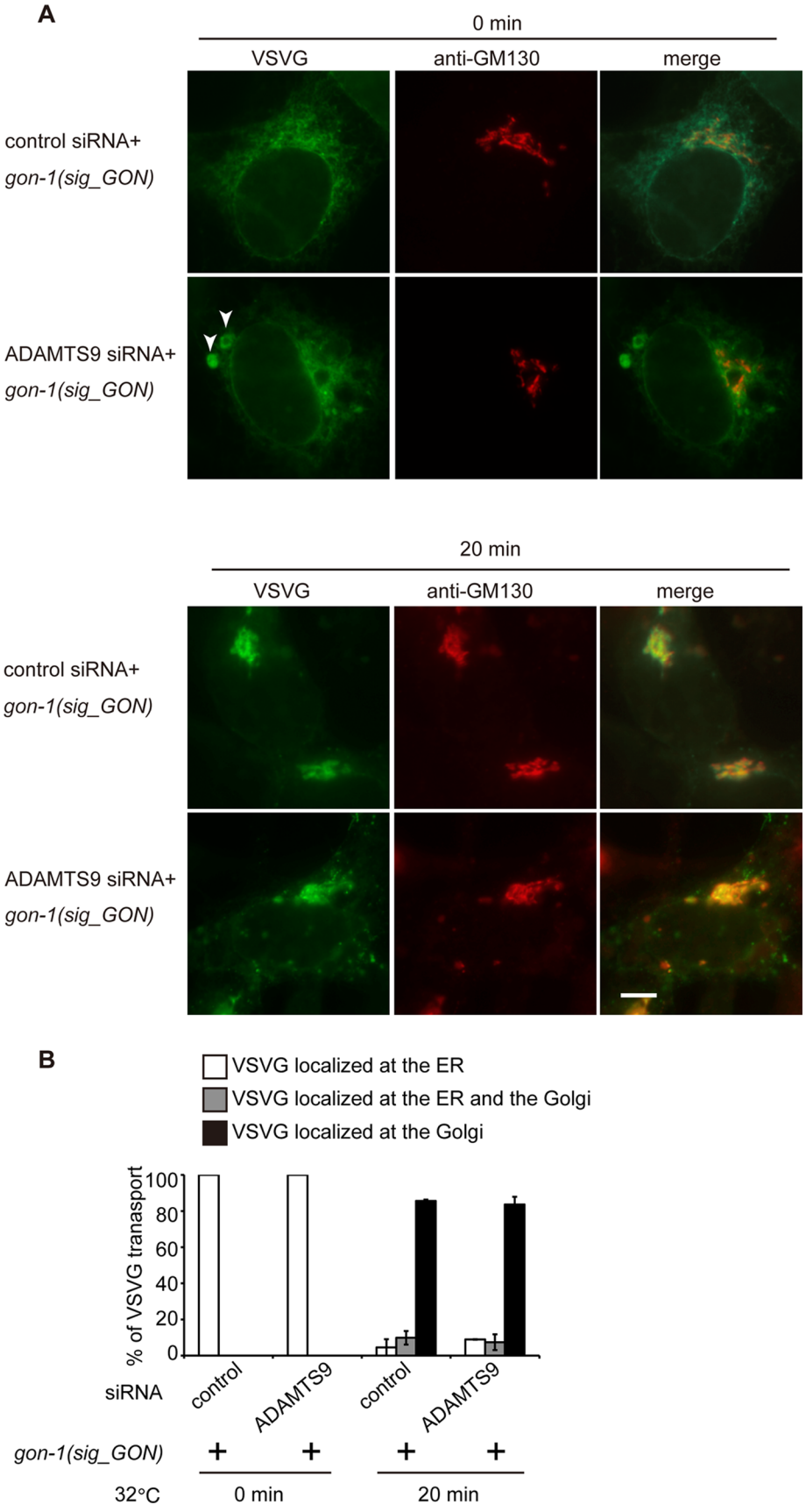

FIGURE 6: The GON domain is important for VSVG transport from the ER to the Golgi in mammalian cells. (A) VSVG- and *gon-1(sig_GON)*–expressing cells were incubated for 16 h at 40°C and then shifted to 32°C. The cells were fixed at the indicated time points following transfer to the permissive temperature. An anti-GM130 antibody labels the Golgi apparatus (middle). VSVG-GFP was transported from the ER to the Golgi by *gon-1(sig_GON)* expression in both the ADAMTS9 siRNA– and control siRNA–treated cells. Scale bar, 5 μm. (B) Quantification of the VSVG transport. The graph represents the combined results of three independent experiments (n > 50 for each experiment). Bars represent mean ± SE.

secretory pathway. Endo H cleaved all the carbohydrate chains of AAT that remained within the cells in both control and ADAMTS9 siRNA–treated cells (Supplemental Figure S16C, Cell). On the other hand, irrespective of siRNA treatment, secreted AAT was Endo H resistant due to the oligosaccharide modification that occurred in the Golgi apparatus (Supplemental Figure S16C, Medium). Thus glycosylation was not affected by ADAMTS9 siRNA treatment.

To examine whether ADAMTS9 is required for ER-associated degradation (ERAD) in the ER, we transfected an ATT variant, null Hong Kong (NHK), which fails to be transported to the Golgi and is degraded by ERAD (Hosokawa *et al.*, 2003), in HEK293 cells. We examined the time course of the degradation of the NHK variant in a cycloheximide-chase experiment with or without ADAMTS9 siRNA. Degradation of the NHK variant did not differ between cells treated with ADAMTS9 siRNA and control siRNA (Supplemental Figure S16D). This finding suggested that degradation of AAT(NHK) by ERAD is not dependent on ADAMTS9.

DISCUSSION

Distal tip cells and body wall muscle cells express *gon-1*, which encodes a ADAMTS-like metalloprotease that functions in ECM remodeling (Jones and Riley, 2005). The *gon-1* gene has an essential role in gonad development in *C. elegans* (Blelloch and Kimble, 1999). The present study revealed that *C. elegans* GON-1, an ADAMTS9 homologue, and human ADAMTS9 also have another function. GON-1 and ADAMTS9 are involved in the mechanisms of protein transport from the ER to the Golgi. In addition, the GON domain at the C-terminus of GON-1 and ADAMTS9 localizes to the ER, and the GON domain is important for ER functions.

In *C. elegans*, down-regulation of *gon-1* led to ER deformation and gonad proliferation defects, and these phenotypes were rescued by GON-domain expression without the protease domain in the ER of DTCs. To investigate whether the role of the GON domain in the ER of DTCs is sufficient for gonad proliferation, we compared transgenic animals harboring two

transgenes—*gon-1(sig_GON)* in DTCs and *gon-1(FL)* in muscle—with transgenic animals harboring only the *gon-1(sig_GON)* in DTCs or with transgenic animals harboring *gon-1(FL)* in muscle. Gonad proliferation recovered to a greater extent in transgenic animals harboring both transgenes—*gon-1(sig_GON)* in DTCs and *gon-1(FL)* in muscle—than in transgenic animals harboring only the *gon-1(sig_GON)* in DTCs or only the *gon-1(FL)* in muscle. Our findings strongly suggest that the GON-1 protein functions both inside and outside DTCs. The GON domain functions in the ER for protein transport from the ER to the Golgi, and at the same time, the protease domain of GON-1 functions outside DTCs to digest ECM proteins. *gon-1(sig_GON)::KDEL,* which has an ER-retention signal, rescued DTC function better than did *gon-1(sig_GON)* in the *gon-1* mutant (Figures 2 and 3). These data support the conclusion that the GON domain acts in the ER.

DTCs are specialized for the stimulation and navigation of gonad proliferation and generate some of the secretory or membrane proteins that are required for gonad navigation, such as UNC-5 (Su *et al.*, 2000), and gonad proliferation, such as LAG-2 (Gao and Kimble, 1995). GPI-anchored proteins are also suggested to be involved in gonad proliferation (Murata *et al.,* 2012). Our data imply that depletion of GON-1 impairs the transport of LAG-2, other germ cell growth factors, and DTC navigation factors to the plasma membrane. For this reason, the gonad of the *gon-1* mutant fails to proliferate and undergo morphogenesis. Future studies to examine the candidate proteins transported by the GON domain function to control gonad proliferation will provide important data.

To elucidate the role of the GON domain, we performed chromophore-assisted light inactivation using the phototoxic fluorescent protein KillerRed and inactivated the GON domain. We observed the time course of the changes in ER morphology and protein secretion inhibition. In the experiments, secretory proteins accumulated in the ER within the early hours after GON-domain depletion. Cells expressing higher levels of membrane proteins contain a number of nonbranching structures, including whorls and open loops (Snapp *et al.*, 2003). Furthermore, the accumulation of VSVG-GFP was observed in both the spherically aggregated, abnormal ER and the mesh-like, normal ER structures in the ADAMTS9 siRNA–treated cells after 20 min at the permissive temperature. These results suggest that the abnormal ER structure might be induced secondarily by the accumulation of proteins in the ER.

In human cells, siRNA-mediated knockdown of ADAMTS9 inhibited transport of the membrane protein VSVG-GFP from the ER to the Golgi and secretion of the secretory proteins PRL-GFP and AAT. Bright oval structures were observed in the ER under the same conditions. Inhibition of protein transport from the ER to the Golgi was recovered by GON-domain expression in the ER. These findings suggest that the GON domain has a common intracellular function: the export of a broader variety of cargo proteins from the ER to the Golgi in human and *C. elegans*.

We searched the Pfam database for proteins from other species that have the GON domain and investigated the size of those proteins, the position of the GON domain, the existence of the signal sequence, TM regions, and the metalloprotease domain. Various species have proteins with the GON domain. The size of those proteins varies from 219 to 2289 residues. Most of them have a signal sequence or a TM region, consistent with the notion that the GON domain is involved in ER-to-Golgi transport and is associated with proteins in the secretory pathway. Those proteins, however, do not necessarily have a metalloprotease or a thrombospondin domain. The metalloprotease domain is not required for GON-domain function, based on the phylogenic origins described earlier, as well as our own observations. The GON domain is present in the most-C-terminal region in these proteins (Supplemental Table S1). These results are consistent with our finding that *gon-1(sig_Venus_GON)* had a higher rescue activity than *gon-1(sig_GON_Venus)*. In addition, the presence of Venus in the C-terminus disrupted the localization of the GON domain in both *C. elegans* and mammalian cells. Thus the C-terminus of the GON domain most likely has an important role in its localization and eventually its function.

Newly synthesized secretory proteins are transported from the ER to the Golgi by COPII-coated vesicles. A large number of proteins, including coat proteins that help vesicle budding, proteins that regulate cargo export, and receptors that bind to secretory cargoes, are required for the biogenesis of COPII-coated vesicles. COPII-coated vesicles comprise the sec23/24 and sec13/31 complexes (Gurkan *et al.*, 2006). Export of cargo proteins from the ER is mediated by sar-1, sec16, and sec12 (Gurkan *et al.*, 2006). TFG-1 regulates cargo export from the ER (Witte *et al.*, 2011). ERGIC-53, Emp24p, surf4, and TANGO1 function as cargo receptors (Nakamura *et al.*, 1998; Muniz *et al.*, 2000; Mitrovic *et al.*, 2008; Nyfeler *et al.*, 2008; Saito *et al.*, 2009). These cargo receptors are believed to mediate cargo loading into COPII vesicles, and the cargo proteins are then exported from the ER to the Golgi. ERGIC-53 has a role in the transport of coagulation factors V and VIII, cathepsin C and Z, and AAT. Emp24p is involved in the transport of Gas1p, a GPI-anchored protein. Surf4 has a role in the transport of soluble proteins. TANGO1 has a role in the transport of collagen VII. These factors are all considered to be involved in transportation of limited types of cargoes. On the other hand, depletion of *gon-1* led to accumulation of TM-EGFP, a TM protein, and a GPI-anchored protein, as well as secretory proteins such as ssVenus, suggesting that the GON domain acts on a variety of cargoes in the secretory pathway. Thus the function of the GON domain appears to differ from those of other transport factors. The amounts and types of cargoes to be transported differ among cell types, but mechanisms of substrate specificity and cell specificity involved in cargo export are not fully elucidated. Of interest, not all cells express GON-1 and ADAMTS9 in the nematode and human, but all cells have some mechanisms of transport from the ER to the Golgi. The dissimilarities among cell types that require the GON domain are not clear. Future studies are needed to elucidate the molecular mechanisms of the action of the GON domain in the ER.

MATERIALS AND METHODS

Nematode strains

The deletion mutant strain of *gon-1(tm3146)* was obtained as described (Gengyo-Ando and Mitani, 2000). The deletion allele was identified by PCR amplification with the primers spanning the deleted region as described in Supplemental Table S2 and Supplemental Figure S2. *gon-1(tm3146)* was derived from the wild-type Bristol strain N2. Genetic crosses were carried out by the standard genetic protocols (Brenner, 1974).

Generation of transgenic strains

The transgenic strains used in this work are listed in Supplemental Table S3. The sequences of the primers for construction of plasmids used for microinjection are listed in Supplemental Table S4. For expression of target proteins in DTC, the promoter region of *lag-2* was amplified by PCR from the *C. elegans* genomic DNA using the primers of plag-2-FW and plag-2-RV and inserted into the pPD95.79 vector plasmid (a gift from A. Fire, Stanford University), giving rise to *pPD95.79_plag-2*. The GFP cDNA that was originally inserted in pPD95.79 was replaced with Venus at *Kpn*I and *Eco*RI sites (*pPD95.79_plag-2::Venus*).

To construct *pmyo-3::gon-1*, the cDNA of *gon-1* was prepared by RT-PCR using the primers of gon-1-FW and gon-1-RV and inserted into *pPD114.95* (a gift from A. Fire) using the *Bam*HI site.

To construct *plag-2::ssVenus* used in Figure 1, a fragment coding for SEL-1–derived signal peptide (ss) was amplified by PCR using the primers of SEL-1-ss-FW and SEL-1-ss-RV. The PCR fragment was inserted into *plag-2::Venus* using the In-Fusion PCR Cloning Kit (Clontech, Mountain View, CA).

To construct *plag-2::C31E10.7::Venus* used in Figure 1 and the *plag-2::lmp-1::Venus and plag-2::aman-2::Venus* used in Supplemental Figure S4, the Venus fragment was inserted into the *pFX_VT* vector plasmid using the *Not*I and *Bgl*II sites, giving rise to *pFX_VT_Venus* (Gengyo-Ando *et al*., 2006). The cDNAs of *C31E10.7*, *lmp-1*, and *aman-2* were amplified by RT-PCR using the primers of C31E10.7-FW and C31E10.7-RV, lmp-1-FW and lmp-1-RV, and aman-2-FW and aman-2-RV, respectively. *C31E10.7* and *lmp-1* cDNA fragments lacking the termination codon were digested and inserted into the *pFX_VT_Venus* vector using the *Not*I site. *aman-2* cDNA fragment (amino acids 1–82) was digested and inserted into the *pFX_VT_Venus* vector using the *Not*I site.

To construct *plag-2::Venus::lgg-1 and plag-2::Venus::rab-5* used in Supplemental Figure S4, the cDNAs of *lgg-1* and *rab-5* were amplified by RT-PCR using the primers of lgg-1-FW and lgg-1-RV, and rab-5-FW and rab-5-RV, respectively. Each cDNA fragment was digested and inserted into the *pFX_VT_Venus* vector using the *Bgl*II site.

To construct *plag-2::Venus::SP12* used in Figure 3, the two separate fragments of *SP12 cDNA* and *Venus* were amplified by PCR using SP12-FW and SP12-RV for *SP12* and Venus-FW and Venus-RV for *Venus* as primers. These fragments were fused together by sewing PCR using Venus-FW and SP12-RV as primers, and the fused fragment was inserted into the plasmid *pPD95.79_plag-2* using the *Bam*HI site.

To construct *plag-2::xbp-1(D81)::Venus* used in Supplemental Figures S6 and S8, the cDNA of the unspliced form of *xbp-1* lacking the nucleotides from 4 to 243 were amplified by RT-PCR using the primers of xbp-1(D81)-FW and xbp-1(D81)-RV and inserted into *pPD95.79_plag-2::Venus* using the In-Fusion PCR Cloning Kit. *xbp-1(D81)* was devoid of the bZIP domain, resulting in the loss of the DNA-binding activity.

To construct *plag-2::gon-1(FL) and plag-2::gon-1(N-TSP12)* used in Figures 2 and 3, the cDNAs of *gon-1(FL)* and *gon-1(N-TSP12)* were amplified by PCR using *pPD114.95_pmyo-3::gon-1* as a template and gon-1-FW2 and gon-1-RV2, and gon-1-FW2 and gon-1(TSP12)-RV, as primers, respectively. To introduce the E425A mutation into the plasmid *plag-2::gon-1*, PCR was performed using a pair of primers specific to the upstream and downstream sequences of a loop tailed with gon-1-mut-FW and gon-1-mut-RV as primers and *pPD95.79_plag-2::gon-1* as a template. After self-ligation with the In-Fusion Kit and plasmid amplification in *Escherichia coli*, the mutation was confirmed by DNA sequencing. To construct *plag-2::gon-1(sig_GON)* used in Figures 2 and 3, the two separate fragments of *gon-1*(base pairs 1–84) and *gon-1*(base pairs 5770–6498) were amplified by PCR using gon-1-FW2 and gon-1(sig)-RV1 for *gon-1*(base pairs 1–84) and gon-1(GON)-FW1 and gon-1-RV2 for *gon-1*(base pairs 5770–6498) as primers and *pPD95.79_plag-2::gon-1* as a template. These fragments were fused together by sewing PCR using gon-1-FW2 and gon-1-RV2 as primers, and the fused fragment was inserted into the plasmid *pPD95.79_plag-2* using the *Bam*HI site.

To construct *plag-2::gon-1(sig_Pro_GON)* used in Figures 2 and 3, the two separate fragments of *gon-1*(base pairs 1–687) and *gon-1*(base pairs 5770–6498) were amplified by PCR using gon-1-FW2 and gon-1(Sig_Pro)-RV1 for *gon-1*(base pairs 1–687) and gon-1(GON)-FW2 and gon-1-RV2 for *gon-1*(base pairs 5770–6498) as primers and *pPD95.79_plag-2::gon-1* as a template. These fragments were fused together by sewing PCR using gon-1-FW2 and gon-1-RV2 as primers, and the fused fragment was inserted into the plasmid *pPD95.79_plag-2* using the *Bam*HI site.

To construct *plag-2::gon-1(sig_Venus_GON)* used in Figures 2 and 3, the three separate fragments of *gon-1*(base pairs 1–84), Venus, and *gon-1*(base pairs 5770–6498) were amplified by PCR using gon-1-FW2 and gon-1(sig)-RV2 for *gon-1*(base pairs 1–84), Venus-FW1 and Venus-RV1 for Venus, and gon-1(GON)-FW3 and gon-1-RV2 for *gon-1*(base pairs 5770–6498) as primers and *pPD95.79_plag-2::gon-1* as the template. These fragments were fused together by sewing PCR using gon-1-FW2 and gon-1-RV2, and the fused fragment was inserted into the plasmid *pPD95.79_plag-2* using the *Bam*HI site.

To construct the *plag-2::gon-1(sig_GON_Venus)* used in Figures 2 and 3, PCR was performed using gon-1-FW2 and gon-1(Δstop)-RV as primers and *pPD95.79_plag-2::gon-1(sig_GON)* as the template. The fragment was inserted into the plasmid *pPD95.79_plag-2* using the *Bam*HI site. To construct *plag-2::gon-1(sig_Pro_Venus_GON)* used in Figures 2 and 3, three separate fragments, *gon-1*(base pairs 1–687), Venus, and *gon-1*(base pairs 5770–6498), were amplified by PCR using gon-1-FW2 and gon-1(sig_Pro)-RV2 as primers for *gon-1*(base pairs 1–687), Venus-FW2 and Venus-RV2 as primers for Venus, gon-1(GON)-FW4 and gon-1-RV2 as primers for *gon-1*(base pairs 5770–6498), and *pPD95.79_plag-2::gon-1* as the template. These fragments were fused together by sewing PCR using gon-1-FW2 and gon-1-RV2 as primers, and the fused fragment was inserted into the plasmid *pPD95.79_plag-2* using the *Bam*HI site.

To construct *plag-2::gon-1(sig_GON_KDEL) and plag-2::gon-1(sig_Venus_GON_KDEL)* used in Figures 2 and 3, PCR was performed using a pair of primers specific to the upstream and downstream sequences of a loop tailed with KDEL-FW and KDEL-RV as primers and *plag-2::gon-1(sig_GON_KDEL)* and *plag-2::gon-1(sig_Venus_GON)* as templates, respectively. The sequences were confirmed by self-ligation with the In-Fusion Kit and plasmid amplification in *E. coli*.

To construct *plag-2::gon-1(sig_KillerRed_GON)* used in Figure 4 and Supplemental Figure S8, the three separate fragments *gon-1*(base pairs 1–84), KillerRed, and *gon-1*(base pairs 5770–6498) were amplified by PCR using gon-1-FW2 and gon-1(sig_KR)-RV as primers for *gon-1*(base pairs 1–84), gon-1(KR_GON)-RV and gon-1-RV2 as primers for *gon-1*(base pairs 5770–6498), gon-1(sig_KR)-FW and gon-1(KR_GON)-RV as primers for KillerRed, and *pPD95.79_plag-2::gon-1* and *pKillerRed-C vector* (Evrogen, Moscow, Russia) as the template. These fragments were fused together by sewing PCR using gon-1-FW2 and gon-1-RV2 as primers, and the fused fragment was inserted into the plasmid *pPD95.79_plag-2* using the *Bam*HI site.

To construct *plag-2::T01F10.1a(TM)::GFP* used in Figure 1, the cDNA of *T01F10.1a(TM)* was amplified by PCR using TM-FW1 and TM-RV1 as primers and inserted into *pPD95.79_plag-2::GFP* using the In-Fusion PCR Cloning Kit.

To construct *pmyo-3::T01F10.1a(TM)::GFP* used in Supplemental Figure S5, cDNA of *T01F10.1a(TM)* was amplified by PCR using TM-FW2 and TM-RV2 as primers and inserted into *pPD114.95* using the In-Fusion PCR Cloning Kit.

To construct *plag-2::YFP-GPI* used in Supplemental Figure S5, YFP-GPI was amplified by PCR using YFP-GPI-FW and YFP-GPI-RV as primers and inserted into *pPD95.79_plag-2* using the In-Fusion PCR Cloning Kit. YFP-GPI was a gift from Tom A. Rapoport (Harvard Medical School).

Microinjection of the described DNA constructs was performed as previously reported (Mello *et al.*, 1991) with appropriate selection markers. Images were taken with a BX-51 microscope (Olympus, Center Valley, PA) or a confocal laser-scanning microscope LSM5 Pascal (Carl Zeiss, Jena, Germany).

RNA interference in *C. elegans*

The feeding RNA interference was performed as previously described (Timmons *et al.*, 2001). Briefly, the *E. coli* strains of HT115(DE3) harboring double-strand RNA expression plasmids were plated on NGM medium containing 1 mM isopropyl-β-D-thiogalactoside and 100 μM ampicillin. At 12 h after plating the bacteria, L1 or L4 larvae were placed on the plates and cultured at 20°C, except for the experiment shown in Supplemental Figure S6C. In Supplemental Figure S6C, the animals were cultured at 12°C to reduce the constitutive activation of *xbp-1*.

RT-PCR analysis

Total RNAs from the worms and HEK293 cells were extracted with the RNeasy Mini Kit (Qiagen, Valencia, CA). Total RNA (5 mg) was used for reverse transcription with the Superscript II reverse transcriptase (Invitrogen, Carlsbad, CA) using the oligo-dT primer and amplified with the *ExTaq* polymerase (TaKaRa, Otsu, Japan) using the primers of sp-xbp-1-FW and sp-xbp-1-RV for the nematode *xbp-1*, sp-XBP1-FW and sp-XBP1-RV for the human XBP1, GAPDH-FW and GAPDH-RV for the human glyceraldehyde-3-phosphate dehydrogenase, and ama-1-FW and ama-1-RV for the nematode *ama-1* (Supplemental Table S5). PCR products were separated on 10% polyacrylamide gels, stained with 5 μg/ml ethidium bromide, and photographed.

Transfection of plasmids and siRNA into HEK293 cells

HEK293 cells were cultured in DMEM media supplemented with 10% fetal bovine serum at 37°C in a humidified 5% CO_2 incubator. Analyses of siRNA-mediated knockdown were performed with ON-TARGETplus SMARTpool L-005779-00 or ON-TARGETplus siCONTROL Non-targeting siRNA (Dharmacon RNAi Technologies, Lafayette, CO) for knockdown of the ADAMTS9 gene or the nontargeting control, respectively. The cells were then transfected with 100 nM siRNA using Lipofectamine 2000 (Invitrogen) and analyzed at 72 h after the transfection.

Plasmids *pCMV_gon-1(sig_GON), pCMV_gon-1(sig_Venus_GON), pCMV_gon-1(sig_GON_Venus), pCMV_ADAMTS9(sig_Venus_GON),* and *pCMV_ADAMTS9(sig_GON_Venus)* were generated by inserting the cDNAs of *gon-1(sig_GON), gon-1(sig_Venus_GON), gon-1(sig_GON_Venus)*, ADAMTS9(sig_Venus_GON), and ADAMTS9(sig_GON_Venus), respectively, into pEGFP-N3 (Clontech). The cDNAs of *ADAMTS9(sig) and ADAMTS9(GON)* were prepared by RT-PCR using the primers of ADAMTS9(sig)-FW and ADAMTS9(sig)-RV, and ADAMTS9(GON)-FW and ADAMTS9(GON)-RV, respectively.

To analyze the localization of GON domain fused with Venus, 1.6-μg plasmids of *pCMV_gon-1(sig_Venus_GON), pCMV_gon-1(sig_GON_Venus), pCMV_ADAMTS9(sig_Venus_GON)*, or *pCMV_ADAMTS9(sig_GON_Venus)* were transfected into cells cultured in two-well chamber slides (Lab-Tek; Nalge Nunc, Rochester, NY) with Lipofectamine 2000.

pCMV_AAT and *pCMV_NHK* were generated by insertion of the cDNA of *AAT* or *NHK* into a plasmid *pAcGFP* from which AcGCF had been removed (Clontech). AAT and NHK were gifts from Randal J. Kaufman (Sanford-Burnham Medical Research Institute). To construct *pCMV_AAT*, the *AAT* cDNA was amplified using the primers of AAT-FW and AAT-RV. To construct *pCMV_NHK*, the AAT cDNA was amplified using NHK-FW and NHK-RV as primers and *pCMV_AAT* as a template and fused with the In-Fusion PCR Cloning Kit. Aliquots of 200 ng of plasmid were transfected into the cultured cells in 35-mm dishes with Lipofectamine 2000 and analyzed at 24 h after transfection.

pCMV_AAT-Flag was generated by inserting the cDNA of *AAT* into *pCMV_Flag,* which was generated by replacing the AcGFP tag of *pAcGFP* with the Flag tag. To construct *pCMV_AAT-Flag*, the AAT cDNA was amplified using AAT-Flag-FW and AAT-Flag-RV as primers. Seventy-two hours after the ADAMTS9 or control siRNA transfection, the cells were transfected with *pCMV_AAT*. Aliquots of 200 ng of plasmid were transfected into cultured cells in 35-mm dishes with Lipofectamine 2000 and analyzed at 24 h after transfection.

pCMV_PRL-GFP was generated by inserting the signal sequence of *PRL* into *pAcGFP* (Voigt *et al.*, 1996). Aliquots of 200 ng of plasmid were transfected into cultured cells in 35-mm dishes with Lipofectamine 2000 and analyzed at 24 h after transfection.

Visualizing the endoplasmic reticulum

To stain the HEK293 cells with an ER-Tracker, the cells were cultured with 100 nM ER-Tracker Blue-White DPX (Invitrogen) in the culture media for 30 min at 37°C with 5% CO_2. After washing with phosphate-buffered saline (PBS), the cells were observed by a microscope with a 40× water-immersion objective. Images were taken with a BX-51 microscope (Olympus) with an epiluminescence light source.

VSVG trafficking

To analyze the protein transport from the ER to the Golgi, with or without the GON-domain function, 1.6 μg of VSVG-GFP (a gift from J. Lippincott-Schwartz, National Institutes of Health) and 0.1 μg of *pCMV_gon-1(sig_GON)* were transfected into the cells cultured in two-well chamber slides (Lab-Tek) with Lipofectamine 2000.

Cells were transfected with VSVG-GFP ts045 (a temperature-sensitive mutant of the VSVG protein) and incubated at 40°C for 16 h. To follow VSVG transport through the secretory pathway, the cells were transferred to 32°C, and after 20 min they were fixed with 4% paraformaldehyde and imaged using fluorescence microscopy.

Transmission electron microscopy

Transmission electron microscopy (TEM) analyses of *C. elegans* were performed as previously described (Maruyama *et al.*, 2005). In brief, the worms were anesthetized in M9 buffer with 8% ethanol for 5 min and then cut into two or three pieces in the primary fixative solution (2% glutaraldehyde, 1% paraformaldehyde, 50 mM sodium cacodylate, 200 mM sucrose, 1 mM $MgCl_2$, pH 7.4). After primary fixation for 2 h at room temperature, the pieces were postfixed in the primary fixative solution with 1% osmium tetroxide and incubated on ice for 2 h. They were then stained en bloc with 2% uranyl acetate for 2 h and dehydrated in a graded ethanol series. After replacement of ethanol with methyl methacrylate, samples were embedded in Rigolac mixture (Tamura and Kushida, 1960). Thin sections were stained with uranyl acetate and lead citrate and subjected to electron microscopic observations using one-slot copper grids precoated with Formvar. The prepared samples were observed with an H-7000 transmission electron microscope (Hitachi, Tokyo, Japan) at 75 keV.

TEM analyses of HEK293 cells were performed at the Hanaichi Ultrastructure Research Institute (Okazaki, Japan). Control siRNA–treated cells or ADAMTS9 siRNA–treated cells were fixed with 2% glutaraldehyde in 100 mM phosphate buffer, postfixed in osmium tetroxide at 4°C, dehydrated, and embedded in EPON812.

Ultrathin sections were analyzed using a transmission electron microscope (JEM-1200EX; JOEL, Peabody, MA) at 80 keV.

Immunostaining

HEK293 cells were plated on chamber slides ~24 h prior to transfection. Twenty-four hours after transfection, the cells were fixed with 4% paraformaldehyde for 10 min at room temperature and permeabilized with 0.1% Triton X-100 for 2 min. The cells were then blocked with PBS containing 5% bovine serum albumin (BSA). The cells were incubated with primary antibodies for 1 h, washed, incubated with the secondary antibodies conjugated with Alexa 488 or 594 for 1 h, washed, and observed. Images were taken with a BX-51 microscope (Olympus) and a confocal laser-scanning microscope LSM5 Pascal (Carl Zeiss). Antibodies were purchased from the following companies: anti-GM130 (BD Biosciences, San Diego, CA), anti-calnexin (BD Biosciences), anti-KEDL (Enzo Life Sciences, Plymouth, PA), and anti-AAT (Dako, Glostrup, Denmark). Secondary antibodies for immunostaining were obtained from Invitrogen.

Immunostaining of DTC was performed as previously described (Maruyama *et al.*, 2005). In brief, transgenic animals that expressed *plag-2::gon-1(sig_Venus_GON)* were placed on a subbed slide in 5.0 ml of M9 containing 1 mM levamisole. Heads or tails were cut off using a 25-gauge needle, extruding the gonad and intestine. Cut animals were fixed with 1.0% paraformaldehyde in PBS for 10 min and permeabilized with PBS containing 0.1% Triton X-100 for 3 min. Samples were blocked in PBS containing 2.5% BSA for at least 30 min. Fixed worms were incubated with an anti-HDEL antibody (Santa Cruz Biotechnology, Santa Cruz, CA) overnight at 4°C. Samples were washed three times with PBS containing 0.5% BSA, incubated with a secondary antibody conjugated with Alexa 594 for 1 h, washed, and observed. Images were taken with a confocal laser-scanning microscope LSM5 Pascal (Carl Zeiss).

Western blotting

Cell lysates were separated by 10% SDS–PAGE. Proteins were blotted onto a polyvinylidene fluoride membrane in blotting buffer (Bio-Rad, Hercules, CA). After blocking in 1% Blocking Reagent (Amersham-Pharmacia Biotech, GE Healthcare Bio-Sciences, Piscataway, NJ), specific proteins recognized by each antibody were detected using ECL reagents (Pierce, Thermo Fisher Scientific, Rockford, IL) and LAS-3000 mini (FujiFilm, Tokyo, Japan). Tubulin was detected by an anti-tubulin antibody (Sigma-Aldrich, St. Louis, MO). AAT-Flag was detected by an anti-Flag antibody (M2; Wako, Osaka, Japan). AAT(NHK) was detected by an anti-AAT antibody (Dako). Secondary antibodies for Western blotting were from Jackson ImmunoResearch Laboratories (West Grove, PA).

Cycloheximide chase experiment

For analysis of AAT(NHK) degradation, HEK293 cells were transfected with pCMV-NHK. After 24 h, transfected HEK293 cells were treated with 10 μg/ml cycloheximide for 0, 1, and 2 h. Protein degradation was examined by Western blotting with an anti-AAT antibody described earlier. The amounts of the NHK protein were normalized by the α-tubulin expression as an internal control.

Immunoprecipitation

Immunoprecipitation was performed by adding protein A Sepharose beads (GE Healthcare, Piscataway, NJ) to the cell extracts, incubating for 1 h in a cold room, and washing with Tris-buffered saline (TBS; 150 mM NaCl, 50 mM Tris-HCl, pH 7.5) buffer. After precipitation of protein A Sepharose beads, the supernatants were collected in other tubes. Anti–flag M2-agarose beads (Sigma-Aldrich) were then added to the supernatants and incubated for 4 h in a cold room, washed with TBS buffer, and resuspended in the sample buffer for SDS–PAGE.

Endo H treatment

Cell extracts were denatured with 1X Glycoprotein Denaturing Buffer at 100°C for 10 min. After adding 1× G5 Reaction Buffer, 500 U of Endo H (New England BioLabs, Ipswich, MA) was added, and the reaction mixture was incubated for 1 h at 37°C. Separation of reaction products was visualized by SDS–PAGE and Western blotting as described.

Chromophore-assisted light inactivation

For photoinactivation experiments, *gon-1(tm3146) mutants* expressing *plag-2::gon-1(sig_KillerRed_GON)* and *plag-2::C31E10.7::Venus, plag-2::ssVenus or plag-2::xbp-1(D81)::Venus* were exposed to a light-emitting diode array (572 nm) for 0, 2, 5, 10, and 24 h after the L4 stage. Transgenic animals were observed on the slide at the indicated time points, and then they were recovered from the slide to NGM plates at 20°C. The time course of the morphological changes of the ER was observed using the transgenic animals that expressed *plag-2::C31E10.7::Venus*. We defined an abnormal ER morphology as one that was observed as a bright fluorescent circular structure with a diameter of 1 μm or larger (Figure 4, B and C). Time courses of the accumulation of secretory proteins were observed using the transgenic animals that expressed *plag-2::ssVenus*. We used an oil-immersion objective with a 100× magnification and recorded the images with a DP30 charge-coupled device camera (Olympus) using a 500-ms exposure time in all of the experiments. We measured the fluorescence intensity using the ImageJ (National Institutes of Health, Bethesda, MA; Figure 4, D and E). The time course of the *xbp-1* splicing was observed using the transgenic animals that expressed *plag-2::xbp-1(D81)::Venus*. We used an oil-immersion objective with a 100× magnification and recorded images using a DP30 camera with a 500-ms exposure time. We measured the fluorescence intensity using ImageJ (Supplemental Figure S9).

ACKNOWLEDGMENTS

We thank S. Endo (University of Tokyo) for TEM support and D. Xue and members of the Mitani laboratory for discussion; A. Fire for the pPD129.36 and pPD95.79 vectors; Y. Kohara (National Institute of Genetics) for cDNA clones; T. A. Rapoport for the YFP-GPI; J. Lippincott-Schwartz for the VSVG-GFP; and R. J. Kaufman for AAT and NHK. Some of the strains used in this work were provided by the *Caenorhabditis* Genetics Center (University of Minnesota, Minneapolis, MN), which is funded by the National Center for Research Resources of the National Institutes of Health. This work was supported by the Program for Promoting the Establishment of Strategic Research Centers; Special Coordination Funds for Promoting Science and Technology; Ministry of Education, Culture, Sports, Science, and Technology (Japan); and Core Research for Evolutional Science and Technology, Japan Science and Technology Agency, to S.M.

REFERENCES

Bernales S, McDonald KL, Walter P (2006). Autophagy counterbalances endoplasmic reticulum expansion during the unfolded protein response. PLoS Biol 4, e423.

Blelloch R, Anna-Arriola SS, Gao D, Li Y, Hodgkin J, Kimble J (1999). The gon-1 gene is required for gonadal morphogenesis in *Caenorhabditis elegans*. Dev Biol 216, 382–393.

Blelloch R, Kimble J (1999). Control of organ shape by a secreted metalloprotease in the nematode *Caenorhabditis elegans*. Nature 399, 586–590.

Boesgaard TW *et al*. (2009). Variant near ADAMTS9 known to associate with type 2 diabetes is related to insulin resistance in offspring of type 2 diabetes patients—EUGENE2 study. PLoS One 4, e7236.
Brenner S (1974). The genetics of *Caenorhabditis elegans*. Genetics 77, 71–94.
Bulina ME, Lukyanov KA, Britanova OV, Onichtchouk D, Lukyanov S, Chudakov DM (2006). Chromophore-assisted light inactivation (CALI) using the phototoxic fluorescent protein KillerRed. Nat Protoc 1, 947–953.
Calfon M, Zeng H, Urano F, Till JH, Hubbard SR, Harding HP, Clark SG, Ron D (2002). IRE1 couples endoplasmic reticulum load to secretory capacity by processing the XBP-1 mRNA. Nature 415, 92–96.
Clark ME, Kelner GS, Turbeville LA, Boyer A, Arden KC, Maki RA (2000). ADAMTS9, a novel member of the ADAM-TS/ metallospondin gene family. Genomics 67, 343–350.
Dempski RE Jr, Imperiali B (2002). Oligosaccharyl transferase: gatekeeper to the secretory pathway. Curr Opin Chem Biol 6, 844–850.
Fares H, Greenwald I (2001). Genetic analysis of endocytosis in *Caenorhabditis elegans*: coelomocyte uptake defective mutants. Genetics 159, 133–145.
Gao D, Kimble J (1995). APX-1 can substitute for its homolog LAG-2 to direct cell interactions throughout *Caenorhabditis elegans* development. Proc Natl Acad Sci USA 92, 9839–9842.
Gengyo-Ando K, Mitani S (2000). Characterization of mutations induced by ethyl methanesulfonate, UV, and trimethylpsoralen in the nematode *Caenorhabditis elegans*. Biochem Biophys Res Commun 269, 64–69.
Gengyo-Ando K, Yoshina S, Inoue H, Mitani S (2006). An efficient transgenic system by TA cloning vectors and RNAi for *C. elegans*. Biochem Biophys Res Commun 349, 1345–1350.
Grarup N, Andersen G, Krarup NT, Albrechtsen A, Schmitz O, Jorgensen T, Borch-Johnsen K, Hansen T, Pedersen O (2008). Association testing of novel type 2 diabetes risk alleles in the JAZF1, CDC123/CAMK1D, TSPAN8, THADA, ADAMTS9, and NOTCH2 loci with insulin release, insulin sensitivity, and obesity in a population-based sample of 4,516 glucose-tolerant middle-aged Danes. Diabetes 57, 2534–2540.
Gurkan C, Stagg SM, Lapointe P, Balch WE (2006). The COPII cage: unifying principles of vesicle coat assembly. Nat Rev Mol Cell Biol 7, 727–738.
Hosokawa N, Tremblay LO, You Z, Herscovics A, Wada I, Nagata K (2003). Enhancement of endoplasmic reticulum (ER) degradation of misfolded Null Hong Kong alpha1-antitrypsin by human ER mannosidase I. J Biol Chem 278, 26287–26294.
Hurskainen TL, Hirohata S, Seldin MF, Apte SS (1999). ADAM-TS5, ADAM-TS6, and ADAM-TS7, novel members of a new family of zinc metalloproteases. General features and genomic distribution of the ADAM-TS family. J Biol Chem 274, 25555–25563.
Jones GC, Riley GP (2005). ADAMTS proteinases: a multi-domain, multifunctional family with roles in extracellular matrix turnover and arthritis. Arthritis Res Ther 7, 160–169.
Jungers KA, Le Goff C, Somerville RP, Apte SS (2005). Adamts9 is widely expressed during mouse embryo development. Gene Expr Patterns 5, 609–617.
Koo BH, Longpre JM, Somerville RP, Alexander JP, Leduc R, Apte SS (2007). Regulation of ADAMTS9 secretion and enzymatic activity by its propeptide. J Biol Chem 282, 16146–16154.
Kuno K, Kanada N, Nakashima E, Fujiki F, Ichimura F, Matsushima K (1997). Molecular cloning of a gene encoding a new type of metalloproteinase-disintegrin family protein with thrombospondin motifs as an inflammation associated gene. J Biol Chem 272, 556–562.
Maruyama R, Endo S, Sugimoto A, Yamamoto M (2005). *Caenorhabditis elegans* DAZ-1 is expressed in proliferating germ cells and directs proper nuclear organization and cytoplasmic core formation during oogenesis. Dev Biol 277, 142–154.
Mello CC, Kramer JM, Stinchcomb D, Ambros V (1991). Efficient gene transfer in *C. elegans*: extrachromosomal maintenance and integration of transforming sequences. EMBO J 10, 3959–3970.
Mitrovic S, Ben-Tekaya H, Koegler E, Gruenberg J, Hauri HP (2008). The cargo receptors Surf4, endoplasmic reticulum-Golgi intermediate compartment (ERGIC)-53, and p25 are required to maintain the architecture of ERGIC and Golgi. Mol Biol Cell 19, 1976–1990.
Murata D *et al*. (2012). GPI-anchor synthesis is indispensable for the germline development of the nematode *Caenorhabditis elegans*. Mol Biol Cell 1 Feb 2012, doi: 10.1091/mbc [Epub ahead of print].
Muniz M, Nuoffer C, Hauri HP, Riezman H (2000). The Emp24 complex recruits a specific cargo molecule into endoplasmic reticulum-derived vesicles. J Cell Biol 148, 925–930.
Nakamura N, Yamazaki S, Sato K, Nakano A, Sakaguchi M, Mihara K (1998). Identification of potential regulatory elements for the transport of Emp24p. Mol Biol Cell 9, 3493–3503.
Nyfeler B, Reiterer V, Wendeler MW, Stefan E, Zhang B, Michnick SW, Hauri HP (2008). Identification of ERGIC-53 as an intracellular transport receptor of alpha1-antitrypsin. J Cell Biol 180, 705–712.
Porter S, Clark IM, Kevorkian L, Edwards DR (2005). The ADAMTS metalloproteinases. Biochem J 386, 15–27.
Poteryaev D, Squirrell JM, Campbell JM, White JG, Spang A (2005). Involvement of the actin cytoskeleton and homotypic membrane fusion in ER dynamics in *Caenorhabditis elegans*. Mol Biol Cell 16, 2139–2153.
Pourkarimi E, Greiss S, Gartner A (2012). Evidence that CED-9/Bcl2 and CED-4/Apaf-1 localization is not consistent with the current model for *C. elegans* apoptosis induction.. Cell Death Differ 19, 406–415.
Saito K, Chen M, Bard F, Chen S, Zhou H, Woodley D, Polischuk R, Schekman R, Malhotra V (2009). TANGO1 facilitates cargo loading at endoplasmic reticulum exit sites. Cell 136, 891–902.
Schroder M, Kaufman RJ (2005). ER stress and the unfolded protein response. Mutat Res 569, 29–63.
Silver DL, Hou L, Somerville R, Young ME, Apte SS, Pavan WJ (2008). The secreted metalloprotease ADAMTS20 is required for melanoblast survival. PLoS Genet 4, e1000003.
Snapp EL, Hegde RS, Francolini M, Lombardo F, Colombo S, Pedrazzini E, Borgese N, Lippincott-Schwartz J (2003). Formation of stacked ER cisternae by low affinity protein interactions. J Cell Biol 163, 257–269.
Somerville RP, Longpre JM, Jungers KA, Engle JM, Ross M, Evanko S, Wight TN, Leduc R, Apte SS (2003). Characterization of ADAMTS-9 and ADAMTS-20 as a distinct ADAMTS subfamily related to *Caenorhabditis elegans* GON-1. J Biol Chem 278, 9503–9513.
Su M, Merz DC, Killeen MT, Zhou Y, Zheng H, Kramer JM, Hedgecock EM, Culotti JG (2000). Regulation of the UNC-5 netrin receptor initiates the first reorientation of migrating distal tip cells in *Caenorhabditis elegans*. Development 127, 585–594.
Tamura H, Kushida H (1960). The age of the worker in a noisy environment and occupational deafness [in German]. Monatsschr Ohrenheilkd Laryngorhinol 94, 347–350.
Timmons L, Court DL, Fire A (2001). Ingestion of bacterially expressed dsRNAs can produce specific and potent genetic interference in *Caenorhabditis elegans*. Gene 263, 103–112.
Voigt S, Jungnickel B, Hartmann E, Rapoport TA (1996). Signal sequence-dependent function of the TRAM protein during early phases of protein transport across the endoplasmic reticulum membrane. J Cell Biol 134, 25–35.
Witte K, Schuh AL, Hegermann J, Sarkeshik A, Mayers JR, Schwarze K, Yates JR 3rd, Eimer S, Audhya A (2011)TFG-1 function in protein secretion and oncogenesis. Nat Cell Biol 13, 550–558.
Zeggini E *et al*. (2008). Meta-analysis of genome-wide association data and large-scale replication identifies additional susceptibility loci for type 2 diabetes. Nat Genet 40, 638–645.